Hindawi
Advances in Materials Science and Engineering
Volume 2019, Article ID 3597480, 13 pages
https://doi.org/10.1155/2019/3597480

Research Article

Experimental and Analytical Study on Seismic Behavior of Strengthened Existing Single Frame Structures with Exterior Cantilevers

Bo Hu,[1,2,3,4] **Xinyu Wei**,[1,2] **Henglin Lv**,[1,2] **Tribikram Kundu**,[4] **and Ning Li**[1,2]

[1]*State Key Laboratory for Geo-mechanics & Deep Underground Engineering, China University of Mining and Technology, Xuzhou 221116, China*
[2]*Jiangsu Collaborative Innovation Center for Building Energy Saving and Construct Technology, Xuzhou 221116, China*
[3]*Jiangsu Key Laboratory of Environmental Impact and Structural Safety in Civil Engineering, China University of Mining and Technology, Xuzhou 221116, China*
[4]*Department of Civil Engineering and Engineering Mechanics, Aerospace and Mechanical Engineering Department, University of Arizona, Tucson, AZ 85721, USA*

Correspondence should be addressed to Bo Hu; bohu@email.arizona.edu

Received 18 April 2018; Revised 22 June 2018; Accepted 8 July 2018; Published 3 February 2019

Academic Editor: Hugo C. Biscaia

Three single reinforcement concrete (RC) frames, including 1 reference specimen and 2 specimens strengthened with shear walls, were fabricated and subjected to low cyclic loadings, in order to evaluate seismic performances of strengthened single frame structures with exterior cantilevers. Through comparison and analysis of failure mode, hysteretic behavior, skeleton curve, energy dissipation, strength, and stiffness degradation of the tested frames, the validity of the shear wall-based reinforcement method for single frames was verified. Test results indicate that the stiffness and load-bearing capacities of strengthened frames increased considerably in comparison with the reference frame. A "strong column-weak beam" failure pattern was observed on the cantilever side, and the failure of the shear wall was always prior to the column, which can increase the structural redundancy and improve the failure mechanism and seismic performance of an existing single frame.

1. Introduction

School is a densely-populated zone, and meanwhile, students generally lack the consciousness of self-preservation and the ability to escape. Once a school building is damaged severely or collapsed, it may cause a lot of casualties and property losses. Meanwhile, the indirect economic loss caused by structural damage is huge. Due to the importance and particularity of primary and secondary school buildings, more and more school buildings need to be retrofitted through different strengthening techniques. Primary and secondary school buildings in China are restricted by ventilation, lighting, and other functional requirements, and single span multistorey reinforced concrete frame structures are often adopted. Statistics show that 3 to 4 storey buildings constitute the majority of single frames with exterior cantilevers, and the height of each storey is usually of around 3.6 m. The plane layout of this kind of structure is arranged in a straight line, containing 3 to 4 education rooms and a stairwell at one end. The typical dimension of an education room is 7.2 m × 9 m, and the width of the exterior cantilever mostly is 2.4 m [1]. Figure 1 shows the span dimensions and storey's number of a typical single frame school building. This kind of structure has a relatively lower redundancy, lateral stiffness, and its energy dissipation, which can lead to a progressive collapse once a vertical member failed in an earthquake [2–4].

Currently, many seismic retrofit techniques for existing RC frame structures have been developed and studied by researchers around the world. Wang and Sheng [5] analyzed the effect of the number of shear walls on the seismic performance of buildings based on an optimization method and considering shear and torsional deformation of shear walls. Shen and Meng [6] used the method of continuous

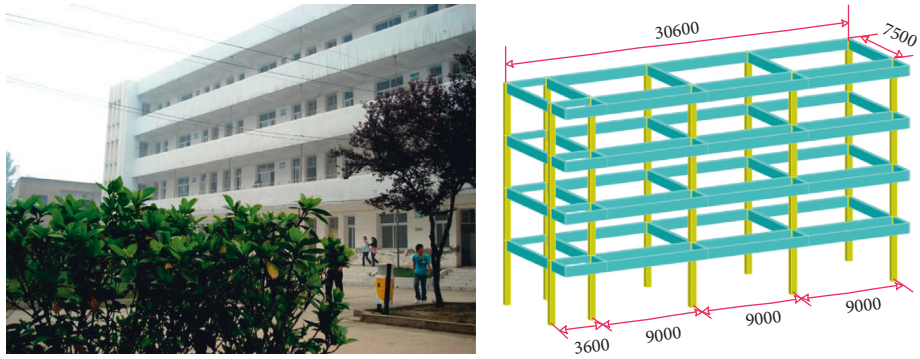

(a) (b)

Figure 1: Span dimensions and number of storeys of a typical school building.

analysis of structural cooperative work. The objective function was the minimum for the structural earthquake action, the optimization model was established with the maximum interlayer displacement angle as the constraint condition, and a reasonable amount of the shear wall with different fortification intensity, site soil category, and design grouping was obtained. Xiong et al. [7] conducted the hysteresis characteristics, energy consumption, and failure mechanism of the RC frame-shear wall structure through pseudodynamic tests. Kaltakci et al. [8] proposed the reinforcement method of the addition external shear wall of the structure and carried out the pseudostatic tests on four frames. The results showed that the reinforcement method could effectively enhance the structural strength and stiffness. Maheri and Ghaffarzadeh [9] evaluated the joints connection strength of the reinforced concrete frame with addition steel braces, and the mutual influences of the bearing capacity of the two systems of the strengthening frame with the addition steel braces and the original frame were analyzed through the test and numerical simulation. El-Sokkary and Galal [10] evaluated the seismic performance of frame structures under frequent, occasional, and rare earthquakes using incremental dynamic analysis (IDA) methods and compared the effects of different strengthening methods on the seismic performance of existing reinforced concrete frame structures. It is pointed out that appropriate reinforcement methods should be comprehensively taken into consideration according to the structural performance, seismic risk, and requirements. Zhou et al. [11] studied the seismic performance of the RC frame with buckling-restrained haunch braces. The results showed that buckling-restrained haunch braces could change the force pattern of the frame structure, so that the plastic hinge was transferred from the beam end and the column end to the connection of the haunch brace, which reduced the force of the beam-column node area and effectively protected the beam-column node. Wu et al. [12] used the method of window-wall reinforcement to strengthen the longitudinal wall of the brick and concrete structure teaching building and compared the difference of the failure mode, bearing capacity, ductility, and energy consumption between the structure after strengthening and the original structure. Zhang et al. [13] proposed the strengthening method of brick walls strengthened with embedded bars, studied the seismic performance of the wall by this method, and gave the calculation formula of the shear bearing capacity of the wall after strengthening.

However, there are few literatures concerning seismic performance of primary and secondary school single frame structures with exterior cantilevers, especially lack of experimental studies. To improve the stiffness, strength, and energy dissipation of the abovementioned existing structures, a novel strengthening strategy was presented in this paper. Meanwhile, three 1/3-scaled test frames of this type (1 reference specimen without strengthening and 2 specimens strengthened with shear walls) were fabricated and subjected to low cyclic loadings, which were used to simulate the earthquake effects. Based on the seismic test results, the hysteresis performance, strength and stiffness degradation, ductility, and energy dissipation capacity of each test frames were analyzed and discussed, and meanwhile, validity of the shear wall-strengthening method for improving the failure mechanism and seismic performance of frames was verified.

2. Experimental Program

2.1. Specimens. In this research, a single span and four storeys RC frame structures with exterior cantilevers was taken as the prototype structure, as shown in Figure 1. A typical substructure with one and a half storeys at the bottom of this building in the transverse direction was selected as the research object, and three test frame specimens were designed and built in a laboratory according to a 1/3 scale. Specimen S1 was the reference model, while specimen S2 and specimen S3 were strengthened with shear walls inside or outside the frames, respectively.

The ratio by weight in which the four ingredients are mixed (water: cement: sand: aggregate) was 0.53 : 1 : 1.25 : 2.73. Based on compressive tests of cubic concrete specimens, the concrete strength was determined as 30.1 MPa. The properties of the reinforcement in the frame are summarized in Table 1, in which f_y and f_u are the yield and ultimate stress, respectively; E_s, δ, and ε_u are the yield, strain hardening, and ultimate strain, respectively.

Table 1: Summary of the properties of reinforcing bars.

Section (mm)	f_y (N/mm^2)	f_u (N/mm^2)	E_s (N/mm^2)	δ (%)	ε_u
ϕ3.5	332	415	2.10 × 105	24	0.1022
ϕ6	276	389	2.03 × 105	26	0.0916
ϕ10	383	521	1.86 × 105	22	0.1209
ϕ12	395	532	1.91 × 105	22	0.1355
ϕ14	387	529	1.87 × 105	23	0.2084

The frame column in the model section size was 150 mm × 150 mm and 165 mm × 165 mm, the beam section size was 100 mm × 230 mm, the floor thickness was 33 mm, the width of each side was 200 mm, the cantilever end length was 800 mm, and a 50 mm diameter circular hole was reserved at the middle of the column in the 2nd storey. The dimensions and reinforcement details are illustrated in Figure 2.

2.2. Test Setup. The schematic diagram of test arrangement and test field photographs is illustrated in Figures 3(a) and 3(b), respectively. The electrohydraulic servoactuator fixed on the reaction wall and steel tie bars were used to apply horizontal cyclic loading to the frame at the middle of the column in the 2nd storey. The holes on the two columns were connected by bolts and steel beams to ensure the effective transmission of the horizontal force and to form a reverse bending point at the middle of the column in the 2nd storey. At the beginning of the test, the column was subjected to a predetermined axial load using hydraulic jacks to keep the axial-compression ratio $N/f_c'A = 0.35$ throughout the test, where N is the axial applied load on the column, f_c' is the cylinder compressive strength, and A is the cross-sectional area of the column. The base beam of the specimen was bolted to the groove, and two jacks were installed between the reaction frame and the base beam to prevent the bottom of the frame from slipping. It should be noted that the positive and negative orientations of the imposed displacement are the south (S) and north (N) directions, respectively, as shown in Figure 3(b).

A hybrid control loading procedure was adopted in this test, which refers to controlling by load prior to yielding and then switching to displacement control [14]. The yielding load of each specimen was determined according to the strain gauges on longitudinal reinforcing bars in the frame; that is, once the reinforcements yielded the corresponding load, displacements were considered as the yielding load and yielding displacement, respectively. Within the displacement loading control phase, magnitude of the imposed displacement increased in multiples of yielding displacement Δ_y, as shown in Figure 4. The load cycle of each stage was two times until the bearing capacity of the specimen dropped to 85% of the peak load, and then, the load was stopped. In this test, measurements include the followings: the development of cracks and the final failure form of the specimens and strain measuring points arranged on the beam end and the column end of the frame node, which used to observe the steel bar strain at these parts; in the frame plane, a total of three displacement gauges were arranged on the storey of one and two and a half height and the foundation beam to measure the horizontal displacement of the frame and monitor the possible slippage of the foundation beam; in addition, two displacement meters are also arranged perpendicular to the plane of the frame to monitor the possible deformation on the out-of-plane of the frame.

3. Experimental Phenomena

3.1. Failure Process of Specimens

3.1.1. Specimen S1. During the loading stage of 30~40 kN, the first crack initiated at the beam end of specimen S1. With the increase of applied load, the number of cracks increased and gradually developed towards the midspan of the beam. During the loading phase of 50~60 kN, cracks on beam bottom penetrated throughout the beam end, and diagonal cracks were eventually formed in the joint zone far from the cantilever side. Within this loading stage, the cracks on the specimen could be closed after unloading. In the 8~16 mm loading stage of displacement control, new cracks appeared at the beam end and in the joint core, and these new cracks were continuously developed. Horizontal cracks appeared inside and outside the column foot. When the displacement increased to 24 mm, the number of cracks on the specimen tended to be stable. Only the initial cracks continued to widen as the applied load increased, and the concrete at the core of the upper end of the column far away from the cantilevered end was slightly crushed. When the displacement reached 32 mm, an X-shaped crack with a maximum width of 3 mm propagated throughout the beam end of the cantilevered side, and the concrete cover was peeled from the core area of the upper end of the column far from the cantilevered end. The number of horizontal cracks of the inner and outer sides at the lower end of the frame column is about 4 to 6 on each side, and it is gradually extended upwards along with the concrete peeling of the column foot. At the end of the experiment, the cracks stayed at 400 mm from the top surface of the foundation. The maximum strain was observed on the longitudinal reinforcements at the beam end, and it was 2207με. The failure pattern of specimen S1 can be attributed to plastic hinges formed at beam ends, as shown in Figure 5(a).

3.1.2. Specimen S2. In the loading stage of 40~60 kN, the first crack appeared in specimen S2, and it was located near the cantilever side beam-wall interface. During the loading process of 70 kN~80 kN, the cracks in the beam end increased significantly, the slender cracks appeared on the bottom of the shear wall at the side of the cantilever, and the number of the cracks increased continuously. In the 120~140 kN loading stage, the end of the beam had a forward and reverse diagonal crack interwoven into a "X" shape, which could not be completely closed after unloading, and the width was about 0.5 mm at the most width. In the stage of displacement control, when the displacement was in the stage of 5.5~11 mm, the reverse diagonal cracks in the beam ends increased, and the concrete on the outer side of the column base spalled. When the displacement was increased

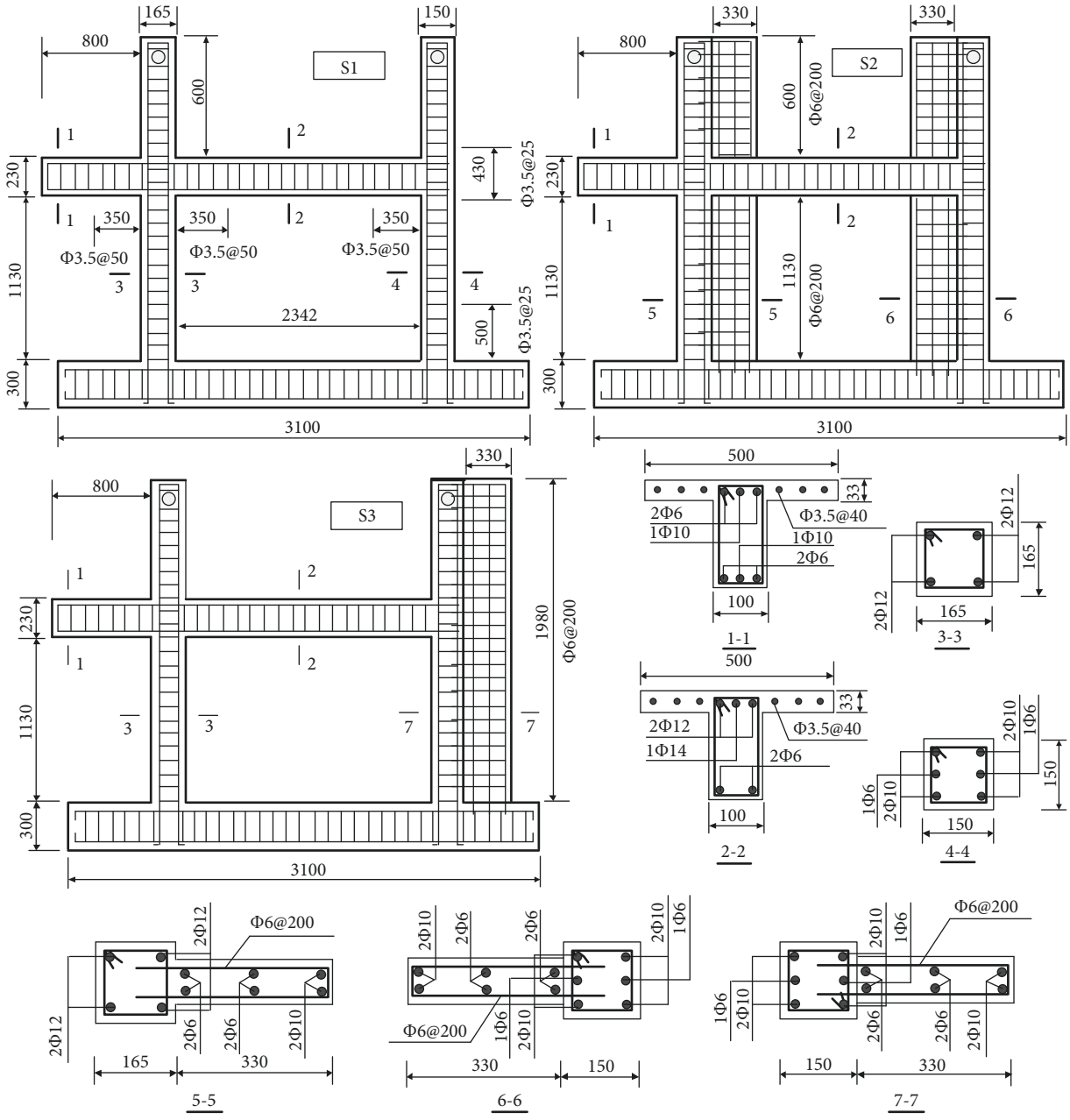

Figure 2: Dimensions and reinforcing details of specimens.

to 16.5 mm, the "X"-shaped cracks at the end of the beam penetrated the whole section, the width was up to 2 mm, and the plastic hinge at the end of the beam was basically formed. After the displacement reached 22 mm, the width of the main crack at the beam end was about 3 mm, the concrete near it spalled, the new diagonal crack appeared at the bottom of the shear wall, and horizontal cracks appeared on the column base on the side of the cantilever. After 27.5 mm loading, the concrete at the inner bottom of the shear wall collapsed, the bare steel yielded, and the interface between the wall and column showed obvious slip. The experiment was finally completed at the loading stage of 33 mm. At this time, the beam end, the bottom of the shear wall, and the column base spalled seriously. There were 3 to 4 horizontal cracks on each side of the frame column, distributed in the range of about 350 mm from the top surface of the foundation. During the whole test, the maximum recorded strain was 3190 $\mu\varepsilon$, which was measured on the reinforcements at the bottom of the newly added shear wall. The final failure pattern of specimen S2 is shown in Figure 5(b), which could be mainly ascribed to the shear failure occurred at the bottom of added shear walls.

3.1.3. Specimen S3. During the loading process of 20~30 kN, the first crack appeared in the vertical direction of the beam end of S3. In the loading stage of 40~50 kN, the cracks at the beam end increased continuously, especially at the side of the

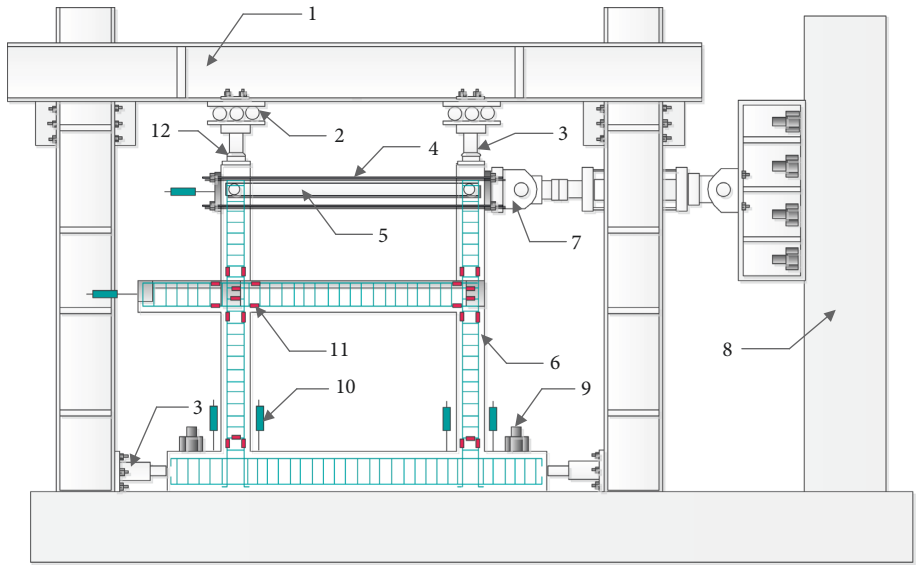

(a)

(b)

Figure 3: Experimental setup: (a) schematic diagram of test arrangement; (b) test field photographs. Note: 1, counterforce frame; 2, sliding vehicle; 3, jack; 4, steel tension rod; 5, angle steel coupling beam; 6, frame specimen; 7, electrohydraulic servoactuator; 8, reaction wall; 9, anchor bolt; 10, LVDT; 11, strain gauge; 12, load cell.

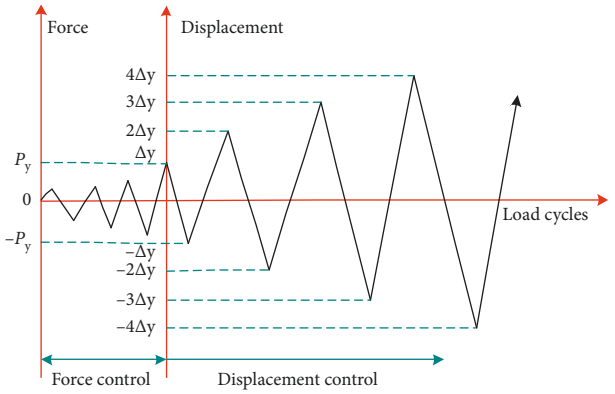

Figure 4: Test loading history.

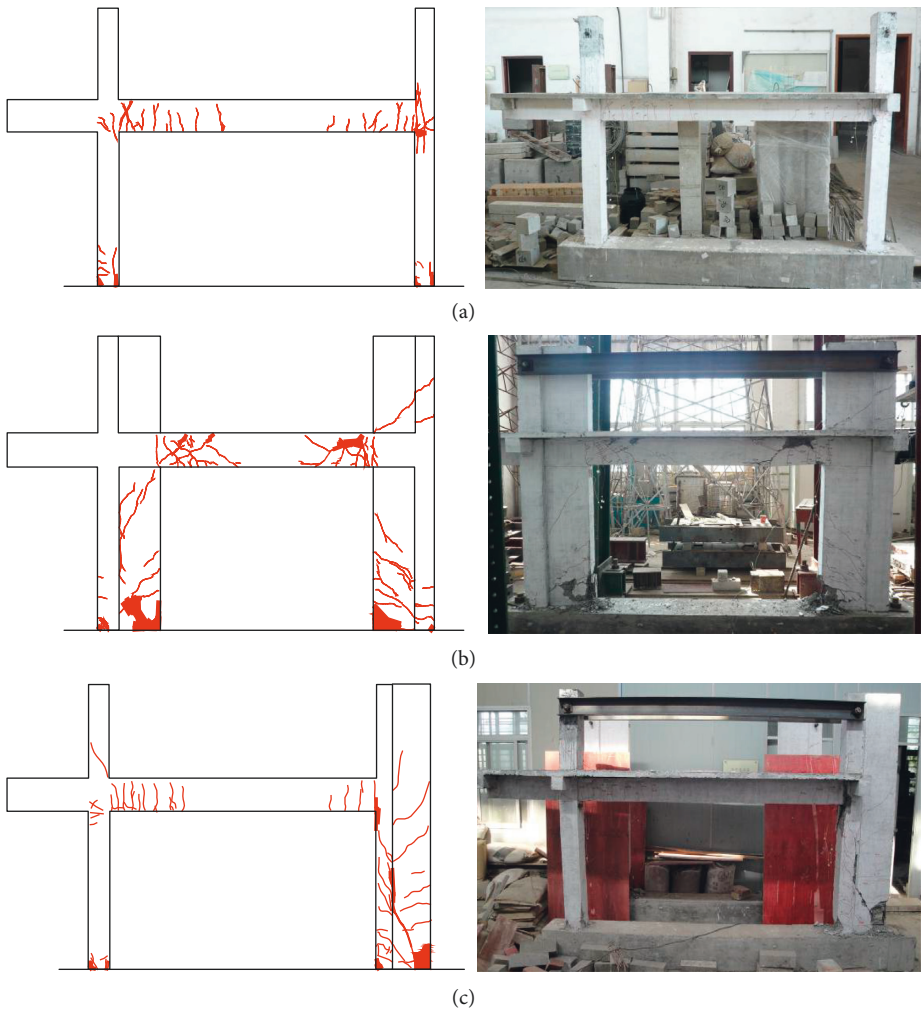

Figure 5: Photographs and crack patterns of specimens after the test: (a) specimen S1; (b) specimen S2; (c) specimen S3.

beam near the cantilevered end. When loading to 50 kN, horizontal cracks appeared at the bottom of the shear wall. In the loading stage of 60~90 kN, diagonal cracks along the 30° direction appeared at the bottom of the shear wall. At this stage, the cracks on the specimen were smaller and could be closed after unloading. In the 5.5~11 mm displacement loading stage, the original crack widened and lengthened, and there were no new cracks. When entering the 12~16.5 mm loading stage, there were new horizontal cracks in the inner and outer sides of the frame column, with 45° of diagonal cracks in the middle of the shear wall and extending to the column. After the completion of the 22 mm displacement loading, diagonal cracks extending from the corner of the wall to the inside of the column with a width of 1.5 mm were formed on the shear wall, and the concrete damage at the corner of the wall was serious. The displacement increased to 27.5 mm, the widest part of the diagonal crack at the corner of the shear wall reached 2 mm, where the concrete cracked continuously and peeled until the steel was buckled, and column base and upper concrete cover had the crisp peeling. When the displacement reached 33 mm, the concrete on the inner of the column base of the shear wall side collapsed, the specimen was destroyed, and the loading was completed.

Figure 5(c) shows the failure pattern of specimen S3 at the end of the test, which also could be classified as the shear failure mode appeared at the bottom of shear wall. Like the abovementioned specimen S2, the maximum strain (2764 $\mu\varepsilon$) on specimen S3 was also measured on the reinforcements at the bottom of the shear wall.

3.2. Failure Characteristics. The failure of specimen S1 can be mainly attributed to the yielding of the beam near the cantilevered end side, and the concrete on the top of the frame column away from the cantilevered side was crushed and spalled off. The concrete cover at the frame column base was peeled off, and the longitudinal reinforcement was buckled. The cantilevered side showed "strong column-weak beam"-type failure, i.e., the beam end first formed a plastic hinge, and then a plastic hinge was formed at the column base, and on the contrary, the plastic hinge was formed closer to the upper end of the column, and then a plastic hinge was formed on the column base.

The damage of test piece S2 mainly showed the beam end section between shear walls first yielded, then the main horizontal load was borne by the shear wall, the concrete was

crushed and peeled on the bottom of the shear wall under the action of the horizontal load, and the longitudinal reinforcement was flexed at the end of the wall. The failure mechanism showed that the plastic hinge was formed at the end of the beam firstly, and then the bottom of the shear wall was destroyed, which ultimately led to a large reduction in the bearing capacity of the frame and damage.

The main failure of specimen S3 was manifested with the cyclic loading of the load, the concrete cover at the bottom of the shear wall was peeled off, the concrete was crushed, and the corresponding longitudinal reinforcement of the wall was buckled. At this time, the tested frame still had a certain bearing capacity. The damage of the frame column near the shear wall side was more serious and finally formed a plastic hinge, and the column also appeared more severely damaged. In the test, the frame beam and cantilevered side frame column were damaged slightly, and there was no obvious plastic hinge at the ends, but the cracks on the cantilevered side beam end were dense, indicating that the location was much weaker than the side frame column. Because the shear wall bore most of the horizontal forces in the early stage of loading, it was first destroyed during the loading process, which constituted the first seismic line of the structure, and then the column base and the column body near the shear wall side are severely damaged, resulting in the frame bearing serious decline.

4. Experimental Results and Analysis

4.1. Hysteretic Curves and Skeleton Curves. Figure 6 shows the force-displacement hysteresis curves of the tested 3 frames, it could be seen that, before cracking, there were only several microcracks in each frame, each frame was in the elastic working state, and the relationship between force and displacement was linear. The hysteresis curves had the following characteristics: the area of the hysteresis curve and structural energy dissipation was quite limited, the stiffness degradation of the structure was not obvious, as well as the residual deformations on frames after unloading.

When entering the elastic-plastic stage, the hysteretic curves of each frame began to change from straight line to arch and gradually moved towards the displacement axis. The area surrounded by hysteresis curves increased gradually, and larger deformation after unloading could not be recovered. There was only a shear wall on the outside of specimen S3, and there were large differences between the forward and reverse hysteresis curves, and the tendency of the curve tending to the displacement axis was more obvious when loading in the forward direction. The hysteretic curves of the three frames were all plump, indicating that each frame has a high energy dissipation capacity.

In the last few loading cycles, the hysteresis curve of specimen S1 showed a certain pinch phenomenon, and the hysteretic curve shape remained basically arched, but the pinch of specimens S2 and S3 curves was particularly severe, and the shapes of the curves were inverse S-shaped, which was related to the larger slip of the longitudinal reinforcement on the bottom of the seismic wall. During the same stage loading process, multiple loading cycles caused accumulation of damage on the frame, which in turn led to degradation of frame strength, stiffness, and energy consumption, and these were shown in the hysteresis curves as the maximum load of the next cycle and the hysteresis loop area both being lower than the previous one.

From Figure 7, it can be seen that there are 4 characteristic points on the skeleton curves of the 3 frames, and that was the cracking point, the yield point, the peak point, and the limit point corresponding to bearing capacity fall to 85% of peak load. There was no forward loading limit point on the skeleton curves of specimens S2 and S3. This was because the forward loading was not performed after the frame was destroyed due to reverse loading. For specimens S2 and S3 with additional shear walls, the corresponding load values of each characteristic point were increased compared with specimen S1, and the increase of specimen S2 was the largest, indicating that the addition of shear walls on the inside of the frame could significantly increase the load capacity of the frame. In the initial stage of loading, the skeleton curve of specimen S1 was closest to the displacement axis, while specimens S2 and S3 had larger deflections to the load axis, which meant that the addition of shear wall would greatly increase the initial stiffness of the frame. On the skeleton curves of specimens S2 and S3, there were descending segments and smooth platform segments after the peak load, indicating that the shear wall had the effect of increasing the seismic line of the structure, so that the framework could maintain a certain bearing capacity after the shear wall was destroyed.

4.2. Characteristic Load and Deformability. The characteristic load of each specimen is shown in Table 2. In this table, P_{cr}, P_y, P_{max}, and P_u represented the cracking load, yield load, peak load, and ultimate load of the specimen, respectively, and the corresponding displacements were, respectively, Δ_{cr}, Δ_y, Δ_{max}, and Δ_u.

From Table 2, it could be seen that compared with specimen S1, the cracking load of S3 was slightly increased, the S2 increased the most, and the forward and reverse directions exceeded 30%. The number of shear walls had a great influence on the cracking load of the frame. The stiffness of frame with an additional shear wall increased greatly, so its yield load also had a large increase. The yield load of specimen S2 increased by 2~3 times when the specimen was loaded positively and reversely, while the yield load of S3 was about 1.8 times than that of specimen S1. For the peak load of the specimens, specimens S2 and S3 with the strengthening of the shear wall also increased significantly compared to specimen S1, of which S2 increased the most, and its forward and reverse directions increased by approximately 126% and 141%, respectively. Because specimen S3 only had shear walls on one side, the increase in peak load during loading in both directions was significantly different, with an increase of about 94% in the reverse direction and an increase of only about 29% in the forward direction. The ultimate loads of specimens S2 and S3 were still larger than that of prototype S1, and the forward and reverse directions of specimen S2 were increased by about 1 times, while the

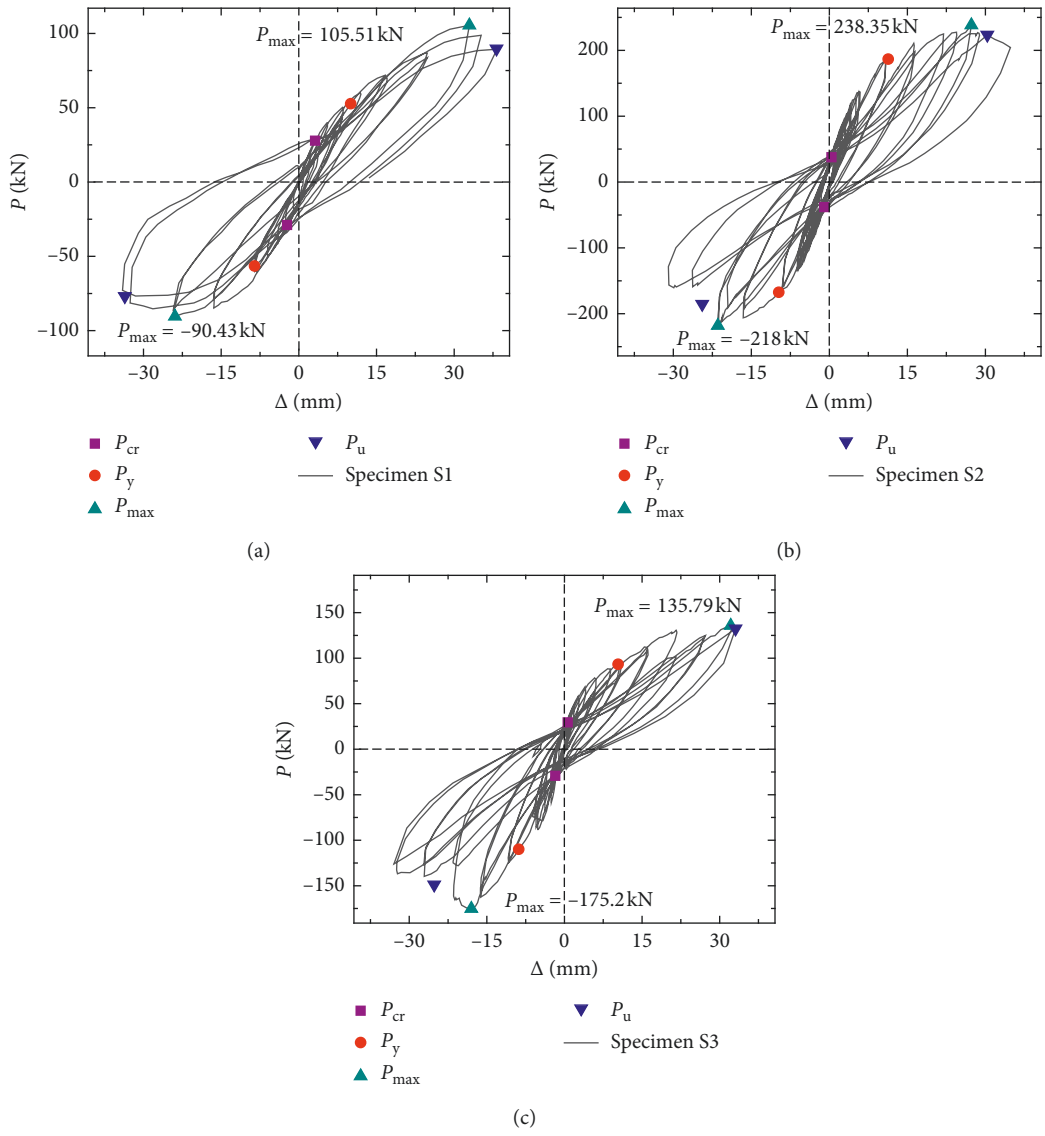

Figure 6: P-Δ hysteretic curves. (a) Specimen S1. (b) Specimen S2. (c) Specimen S3.

forward and reverse directions of S3 were increased by about 50% and 80%, respectively. Table 1 also gave the ductility coefficient of each specimen μ ($\mu = \Delta_u/\Delta_y$). It could be found that the ductility coefficients of specimen S1 were, respectively, 3.81 and 3.93 when loaded in forward and reverse directions, which indicated that the prototype frame has certain ductility. The ductility coefficient of the strengthening frames of S2 and S3 was less than that of specimen S1, and the ductility coefficient of specimen S2 was the least, which indicated that the addition seismic wall would reduce the ductility of the original structure while increasing the structure bearing capacity, and the ductility decreased with the increase of the number of seismic walls.

4.3. Stiffness Degradation. The overall conversion stiffness of the frame was defined as $K_j = P_j/\Delta_j$ [16] to characterize the stiffness degradation of the frame during loading. P_j and Δ_j were the maximum loads and corresponding displacement, which reached by the jth cycle under cyclic horizontal force. The calculated stiffness of each frame variation with the displacement is shown in Figure 8.

It could be seen that the stiffness of each frame was significantly degraded under cyclic loading and the degradation trend was basically consistent. When the specimen was cracked, compared to the initial stiffness, the conversion stiffness of specimen S1 decreased by about 20% to 30%, while specimens S2 and S3 decreased by more than 50%. At the time of yield, the overall conversion stiffness of specimen S1 was about 45% of the initial stiffness, and the values of specimens S2 and S3 were about 20%. When the peak load was reached, the conversion stiffness of specimen S1 was reduced to about 25% of the initial stiffness, while the values of specimens S2 and S3 were only about 10%. The stiffness degradation of the specimens at each characteristic point indicated that the stiffness degradation of each specimen was

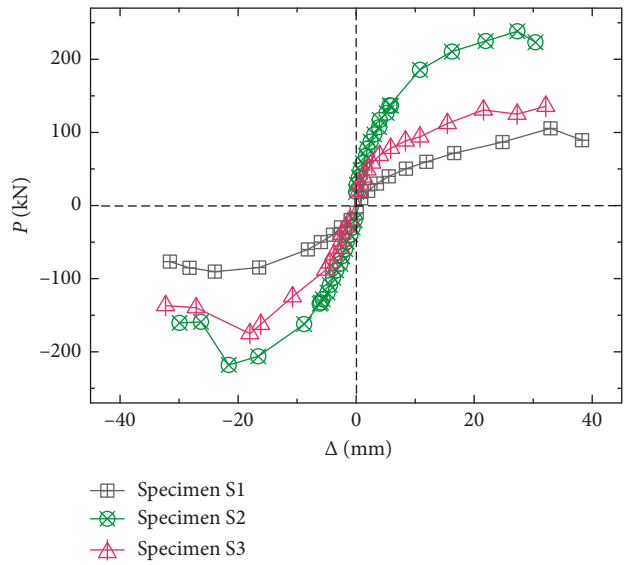

Figure 7: Skeleton curves.

mainly concentrated before yielding, especially when specimens S2 and S3 cracked, the stiffness had been greatly degraded. The stiffness degradation of specimens S2 and S3 after the yielding was significantly slowed down. This was due to the fact that the shear wall restricted the development of horizontal cracks on the column and reduced the damage of the core area of the beam-column node.

4.4. Energy Dissipation Capacity. The energy consumption of each frame under different lateral displacement conditions is shown in Figure 9. It could be seen that the energy consumption of each specimen before cracking was very little, and it was basically zero. With the increase of loading and displacement, the energy consumption of the frame increased continuously, but the energy consumption of each specimen increased slowly before yielding. When the displacement was 10 mm, the energy consumption of each specimen was about 7%, 19%, and 23% of their maximum energy consumption.

After entering the elastic-plastic stage, the energy consumption of each specimen increased rapidly. The corresponding energy consumption of specimens S1, S2, and S3 peak load was 79%, 97%, and 93% of their maximum energy consumption, which indicated that the energy consumption of the frame was less before yielding, and the energy consumption in the elastic-plastic stage was increased significantly. After the failure of the shear wall, the energy curve of specimen S2 appeared the smooth stage, then continued to grow, and its energy consumption was always greater than that of specimen S1, while the energy consumption of specimen S3 decreased first, then increased slightly, and the final energy consumption was lower than that of specimen S1. This was because the side column of specimen S3 was affected by the shear wall attached to it and became the weakest link and was the first to damage and leaded to the failure of the entire structure; however, the damage observed on other parts of specimen S3 was fairly lighter during the whole testing. The test results reported above indicated that the added shear walls in an existing single frame structure can improve its energy dissipation capacity, and the frame strengthened with shear walls inside had the highest increasing extent.

4.5. Restoring Force Model. The restoring force model adopted a stiffness degradation quad-linear restoring force model as shown in Figure 10. The restoring force model had the following characteristics: the forward and reverse skeleton curves of the hysteretic curves are simplified as the quad-linear restoring force model formed by connecting cracking point, yield point, peak point, and ultimate point.

In this restoring force model, the loading stiffness corresponding to each stage is assumed to be the slope of lines, where K_1, K_2, K_3, and K_4 are the equivalent stiffness, respectively, corresponds to cracking, yielding, peak, and ultimate loading stages, and the values of the stiffness are determined using the following equations:

$$K_i = \begin{cases} \dfrac{P_{cr}}{\Delta_{cr}}, & i = 1, \\ \dfrac{\left(P_y - P_{cr}\right)}{\left(\Delta_y - \Delta_{cr}\right)}, & i = 2, \\ \dfrac{\left(P_{max} - P_y\right)}{\left(\Delta_{max} - \Delta_y\right)}, & i = 3, \\ \dfrac{\left(P_u - P_{max}\right)}{\left(\Delta_u - \Delta_{max}\right)}, & i = 4, \end{cases} \tag{1}$$

where P_{cr}, P_y, P_{max}, and P_u are the cracking load, yield load, peak load, and the ultimate load, and Δ_{cr}, Δ_y, Δ_{max}, and Δ_u are the displacements corresponding to the abovementioned applied loads.

Before cracking, stiffness degradation and residual deformation are not considered. After that, the unloading stiffness was determined according to the frame unloading stiffness degradation formula. The stiffness degradation formula for each specimen was obtained using regression analysis of the experiment results, as shown in Figure 11. Logarithmic function was adopted as the fitting function here to regress the stiffness degradation curves, and the regression analysis results are as follows:

$$\begin{aligned} &\text{specimen S1:} \begin{cases} K = -3.3\ln(|\Delta|) + 16.39 & \text{positive loading,} \\ K = -3.72\ln(|\Delta|) + 17.24 & \text{negative loading,} \end{cases} \\ &\text{specimen S2:} \begin{cases} K = -15.18\ln(|\Delta|) + 70.81 & \text{positive loading,} \\ K = -18.67\ln(|\Delta|) + 74.84 & \text{negative loading,} \end{cases} \\ &\text{specimen S3:} \begin{cases} K = -13.51\ln(|\Delta|) + 56.34 & \text{positive loading,} \\ K = -9.281\ln(|\Delta|) + 45.94 & \text{negative loading.} \end{cases} \end{aligned} \tag{2}$$

According to the comparison between the hysteretic curves of the frames determined by the restoring force model

Table 2: Test results.

Specimen	P_{cr}	Δ_{cr}	P_y	Δ_y	P_{max}	Δ_{max}	P_u	Δ_u	P_u/P_{max}	μ
S1	27.84	3.14	52.73	10.03	105.51	32.95	89.68	38.19	0.85	3.81
	−28.92	−2.27	−56.53	−8.56	−90.43	−23.93	−76.87	−33.62	0.85	3.93
S2	37.6	0.41	186.64	11.32	238.35	27.32	223.45	30.38	0.94	2.68
	−38.12	−0.97	−167.33	−9.72	−218	−21.43	−185.3	−24.45	0.85	2.52
S3	29.47	0.64	93.35	10.37	135.79	32.14	132.43	33.08	0.98	3.19
	−29.25	−1.77	−109.91	−8.83	−175.2	−18.00	−148.92	−25.17	0.85	2.85

Note: the cracking load P_{cr} is corresponding to the applied load that once the first crack was observed on the specimen, and the yield load P_y is obtained using the so-called equivalent energy method [15] based on the skeleton curves shown in Figure 7.

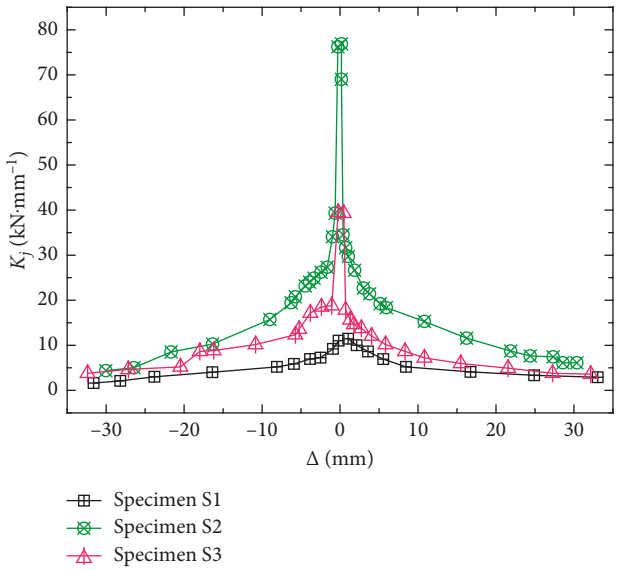

Figure 8: Stiffness degradation curves.

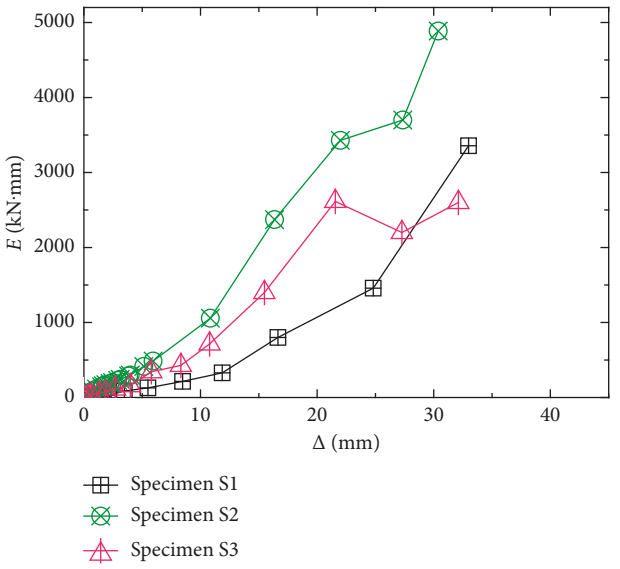

Figure 9: Energy dissipation curves.

and the measured experiment values, it was shown that the restoring force model of the frame under low cyclic loading calculated in this paper agrees well with the experimental results, as shown in Figures 12–14.

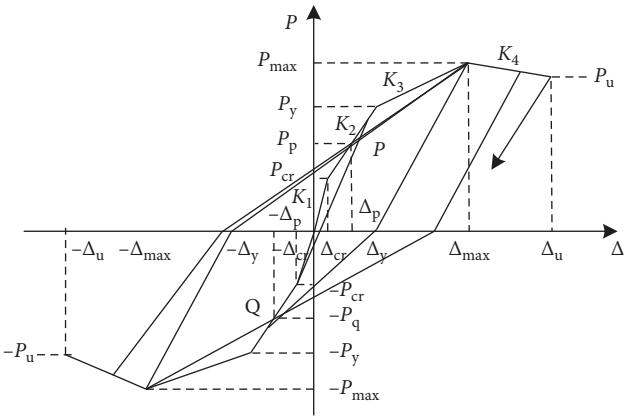

Figure 10: Quad-linear restoring force model.

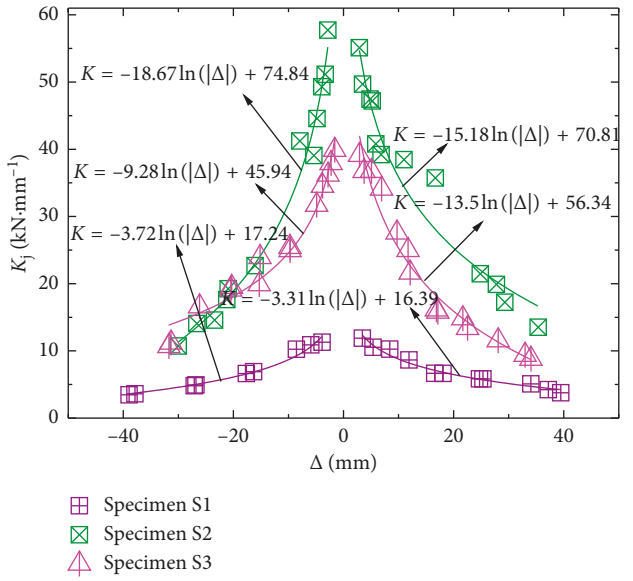

Figure 11: Stiffness degradation calculation.

5. Conclusions

The seismic performance of one comparative frame without strengthened and two frames strengthened with shear walls were studied by the low cyclic loading test. The main conclusions are as follows:

(1) The three frames have obvious differences in stress characteristics, failure process, and failure mechanism

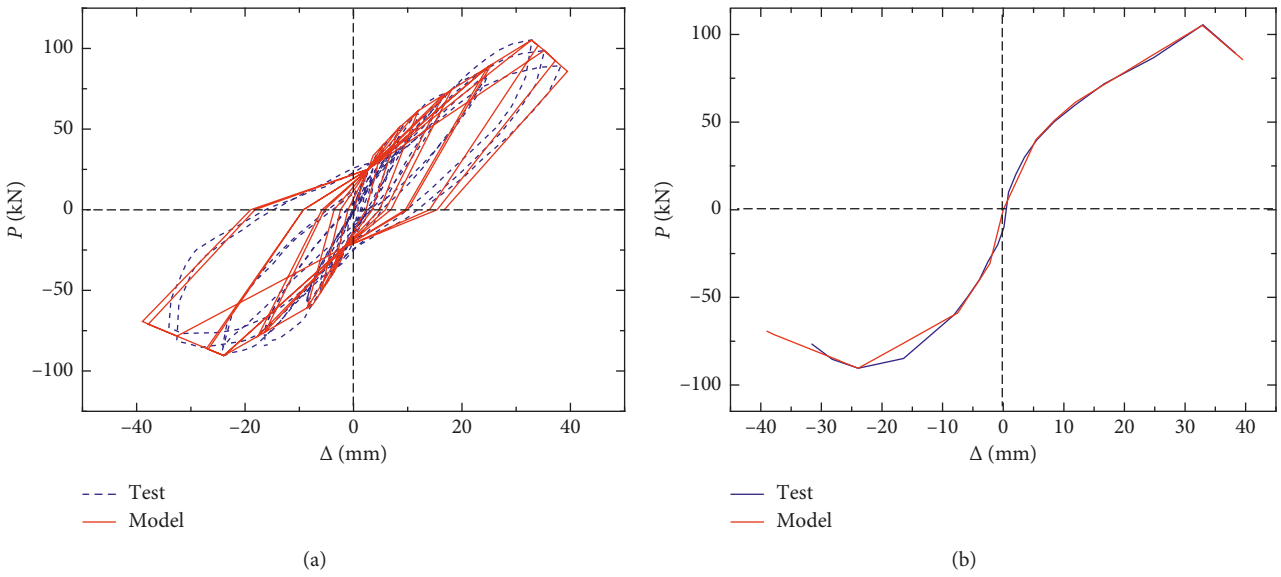

Figure 12: Comparison of the restoring force model and test results of specimen S1: (a) hysteretic curves; (b) backbones.

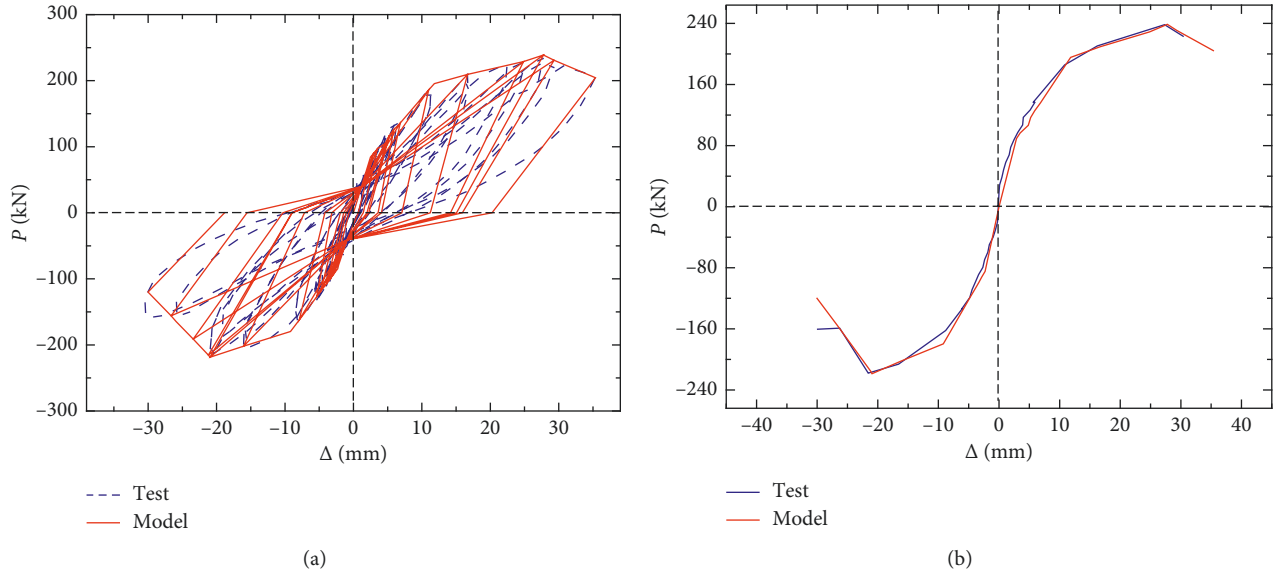

Figure 13: Comparison of the restoring force model and test results of specimen S2: (a) hysteretic curves; (b) backbones.

under low cyclic loading: specimen S1 showed near cantilever end "strong column-weak beam"-type failure and far from the cantilever end column hinges failure; specimen S2 was a "strong column and wall-weak beam"-type of failure, that was, the beam member first appeared plastic hinges, then the shear wall was damaged, and the column hinges appeared at the bottom of the two sides of the column. The seismic wall of specimen S3 was the main lateral force resistant member, and the horizontal force was assumed by the frame after the failure of the seismic wall. Finally, the plastic hinge on the frame column connected to the seismic wall led to the failure of the structure.

(2) The addition of the shear wall can effectively improve the overall stiffness and bearing capacity of the structure. The initial stiffness of specimens S2 and S3 was 6.7 times and 3.4 times as much as that of specimen S1, respectively. Compared with specimen S1, the forward and reverse yield load of specimen S2 increased by 254% and 196%, respectively, and specimen S3 increased by 77% and 94%, respectively. The forward and reverse peak load of specimen S2 increased by 126% and 141%, respectively, and specimen S3 increased by 29% and 94%, respectively.

(3) The ductility coefficients of strengthened frames (i.e., specimens S2 and S3) are between 2.52 and 3.19,

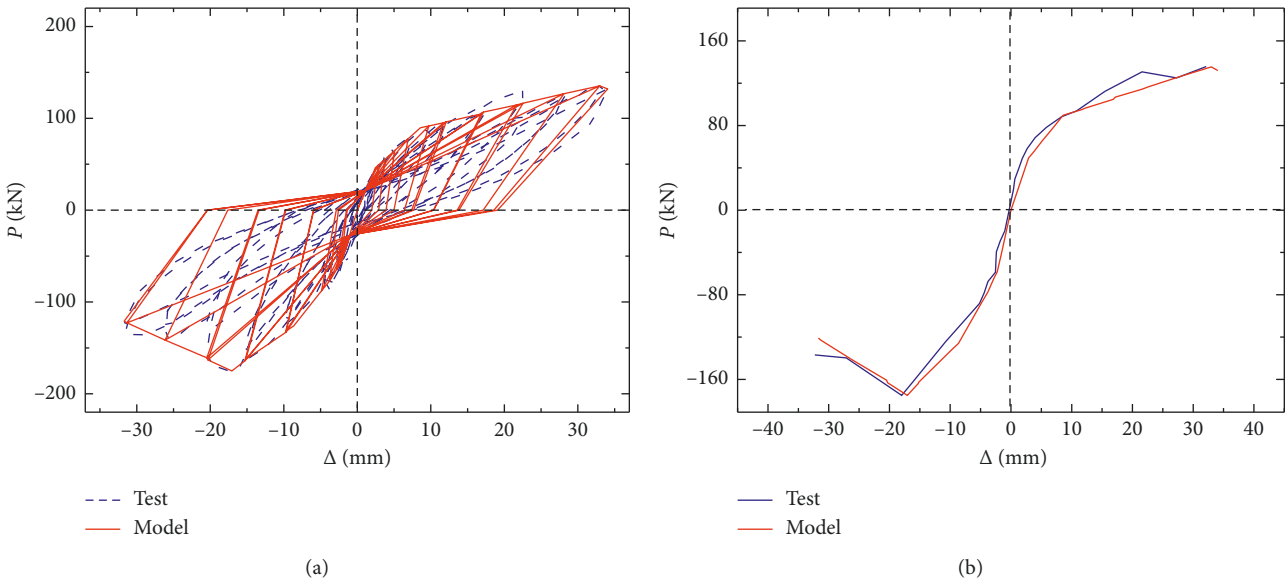

Figure 14: Comparison of the restoring force model and test results of specimen S3: (a) hysteretic curves; (b) backbones.

which are lower than that of the reference frame S1. This indicated that the addition of shear walls would reduce the ductility of frames, and the ductility decline was related to the number of added shear walls. However, the ductility coefficients of strengthened frames are still greater than the recommended target value 2.36 [17].

(4) Before the failure of the shear wall, the energy dissipation capacity of specimens S2 and S3 is greater than that of specimen S1. In the late stage of loading, for specimen S3, the damage degree of the columns connected to the shear walls is far more serious than that in the other parts of the frame. Specimen S3 failed to fully utilize the potential of energy consumption, and the energy consumption was lower than that of specimen S1.

Data Availability

The data used to support the findings of this study were supplied by Bo Hu under license and so cannot be made freely available. However, requests for access to these data are welcome and should be made to Bo Hu (e-mail: bohu@email.arizona.edu). Requests will be considered by the corresponding author then.

Conflicts of Interest

The authors declare that they have no conflicts of interest.

Acknowledgments

The authors acknowledge the financial support of the National Natural Science Foundation of China (Grant No. 51508554) and the Natural Science Foundation of Jiangsu Province (Grant No. BK20150190). Dr. Bo Hu gratefully acknowledges the China Scholarship Council (No. 201706425058) for the financial support of the study at the University of Arizona. The authors also would like to acknowledge the Postdoctoral Science Foundation of Jiangsu Province (No. 1402062C), the Fundamental Research Funds for the Central Universities (No. 2015QNB12), and Jiangsu Collaborative Innovation Center for Building Energy Saving and Construct Technology (sjxtq1523). The financial support is greatly appreciated.

References

[1] Y. L. Xu and Y. Gong, "Investigation of collapse of teaching buildings during the Wenchuan Earthquake: third anniversary memorial of 5·12 Wenchuan Earthquake," *Journal of Building Structures*, vol. 32, no. 5, pp. 9–16, 2011.

[2] D. Wu, S. Tesfamariam, S. F. Stiemer et al., "Comparison of seismic performance of a RC frame building before and after the Wenchuan Earthquake in Sichuan Province," *Journal of Performance of Constructed Facilities*, vol. 29, no. 1, article 04014038, 2015.

[3] T. Guo, W. Xu, L. Song, and L. Wei, "Seismic-isolation retrofits of school buildings: practice in China after recent devastating earthquakes," *Journal of Performance of Constructed Facilities*, vol. 28, no. 1, pp. 96–107, 2014.

[4] B. M. Shahrooz and J. P. Moehle, "Evaluation of seismic performance of reinforced concrete frames," *Journal of Structural Engineering*, vol. 116, no. 5, pp. 1403–1422, 1990.

[5] Q. S. Wang and S. S. Sheng, "Optimal analysis for shear wall quantity of frame-shear wall tall buildings under seismic load," *China Civil Engineering Journal*, vol. 14, no. 3, pp. 1–12, 1981.

[6] S. P. Shen and L. H. Meng, "Optimal quantity of shear wall in frame-shear wall structures based on optimal principle," *Journal of Hunan University (Natural Sciences)*, vol. 33, no. 5, pp. 1–5, 2006.

[7] Z. M. Xiong, X. Q. Shi, S. L. Wang et al., "Hysteretic response and energy dissipation of a model frame-shear wall structure," *Journal of Building Structures*, vol. 27, no. 4, pp. 89–95, 2006.

[8] M. Y. Kaltakci, M. H. Arslan, U. S. Yilmaz, and H. D. Arslan, "A new approach on the strengthening of primary school

buildings in Turkey: an application of external shear wall," *Building and Environment*, vol. 43, no. 6, pp. 983–990, 2008.

[9] M. R. Maheri and H. Ghaffarzadeh, "Connection overstrength in steel-braced RC frames," *Engineering Structures*, vol. 30, no. 7, pp. 1938–1948, 2008.

[10] H. El-Sokkary and K. Galal, "Analytical investigation of the seismic performance of RC frames rehabilitated using different rehabilitation techniques," *Engineering Structures*, vol. 31, no. 9, pp. 1955–1966, 2009.

[11] Y. Zhou, Q. L. Yi, S. M. Lin et al., "Seismic performance investigations of RC frame structures with buckling-restrained haunch braces," *China Civil Engineering Journal*, vol. 45, no. 11, pp. 29–38, 2012.

[12] H. Wu, S. C. Zhao, H. X. et al., "Experimental study on seismic performance of brick-concrete masonry school buildings with wall piers reinforced with anchored reinforcements," *Journal of Building Structures*, vol. 34, no. 4, pp. 49–56, 2013.

[13] G. T. Zhang, K. B. Shi, and Y. J. Li, "Experimental study on seismic behavior of brick walls strengthened with embedded bars," *Journal of Building Structures*, vol. 34, no. 5, pp. 145–150, 2013.

[14] B. Hu, B. K. Liu, and C. G. Wang, "Seismic damage evaluation of recycled concrete frame using wavelet transform," *Applied Mechanics and Materials*, vol. 226–228, no. 29, pp. 1076–1080, 2012.

[15] B. Hu and J. Wang, "Experimental investigation and analysis on flexural behavior of CFSTTC beams," *Thin-Walled Structures*, vol. 116, pp. 277–290, 2017.

[16] B. Hu and T. Kundu, "Seismic performance of interior and exterior beam-column joints in recycled aggregate concrete frames," *Journal of Structural Engineering ASCE*, vol. 145, no. 3, article 04018262, 2019.

[17] J. Cai, Q. Zhou, and X. D. Fang, "Study on seismic displacement ductility factor of reinforced concrete frame structure," *Earthquake Resistant Engineering*, vol. 27, no. 3, pp. 2–6, 2005.